Mixed-valent metallic pyrochlore iridate: A possible route to non-Fermi liquids

Md Salman Khan, Ilaria Carlomagno, Carlo Meneghini, P. K. Biswas, Fabrice Bert, Subham Majumdar, and Sugata Ray

Mixed-valent metallic pyrochlore iridate: A possible route to non-Fermi liquids

Md Salman Khan [1], Ilaria Carlomagno,[2] Carlo Meneghini,[3] P. K. Biswas,[4] Fabrice Bert,[5]
Subham Majumdar,[6] and Sugata Ray [1,7,*]

[1]*School of Materials Science, Indian Association for the Cultivation of Science, 2A and 2B Raja S. C. Mullick Road,
Jadavpur, Kolkata 700032, India*
[2]*Elettra Sincrotrone Trieste, Area Science Park 34149, Basovizza (TS), Italy*
[3]*Dipartimento di Scienze, Universitá Roma Tre, Via della Vasca Navale, 84 I-00146 Roma, Italy*
[4]*ISIS Facility, Rutherford Appleton Laboratory, Chilton, Didcot, Oxon OX110QX, United Kingdom*
[5]*Université Paris-Saclay, CNRS, Laboratoire de Physique des Solides, 91405 Orsay, France*
[6]*School of Physical Science, Indian Association for the Cultivation of Science, 2A and 2B Raja S. C. Mullick Road,
Jadavpur, Kolkata 700032, India*
[7]*Technical Research Center, Indian Association for the Cultivation of Science, 2A and 2B Raja S. C. Mullick Road,
Jadavpur, Kolkata 700032, India*

Non-Fermi liquid behavior in some fermionic systems has attracted significant interest in last few decades. Certain pyrochlore iridates with stronger spin-orbit coupling strength have recently been added to the list. Here, we provide evidence of such a non-Fermi liquid ground state in another mixed-valent metallic pyrochlore iridate $Pb_2Ir_2O_{7-\delta}$, through the combined investigation of electronic, magnetic, and thermodynamic properties as a function of temperature (T) and applied magnetic field (H). Resistivity measurement showed a linear temperature dependence down to 15 K below which it shows $\rho \sim T^{3/2}$ dependence while magnetic susceptibility diverges as $\chi(T) \sim T^{-\alpha}$ ($\alpha < 1$) below 10 K. While a strong negative Θ_{CW} has been observed from Curie-Weiss fitting, the absence of any long-range order down to 80 mK only indicates the presence of strong inherent geometric frustration in the system. Heat capacity data showed $C_p \sim T \ln(T_0/T) + \beta T^3$ dependence below 15 K down to 1.8 K. More importantly spin-orbit coupling strength by x-ray absorption spectroscopy was found to be weaker in $Pb_2Ir_2O_{7-\delta}$ compared to other pyrochlore iridates. In the absence of any large moment rare earth magnetic ion, $Pb_2Ir_2O_{7-\delta}$ presents a rare example of an iridate system showing non-Fermi liquid behavior due to disordered distribution of Ir^{4+} and Ir^{5+} having markedly different strengths of spin-orbit coupling which might offer a prescription for achieving new non-Fermi liquid systems.

I. INTRODUCTION

One of the puzzling phenomena of correlated electronic materials is the understanding of the non-Fermi liquid (NFL) behavior of interacting fermions which goes beyond Landau's Fermi liquid paradigm. Although simple metals could be aptly described by the Fermi liquid (FL) theory, there are several fermionic systems such as spin-orbit assisted Mott insulator [1,2], heavy fermionic systems [3–5], one-dimensional Luttinger liquids [6], and also the high T_c cuprate superconductors [7,8], that cannot be dealt with the same and they are identified as the signature NFL systems. It is now understood that a finite density of fermions directly coupled to a gapless bosonic mode, as is expected near quantum critical points of metals, or two-channel and disordered Kondo systems, or spin-charge separation and the appearance of spinon and holon quasiparticles as observed in one-dimensional Luttinger liquids, are some of the phenomena which can trigger the NFL state [9–14]. On the other hand, disorder induced NFL treated by the disordered Hubbard model away from weak disorder limit [15–17] opens up another possibility, while the recent treatment of random couplings in flavor space between the fermions and the bosonic order parameters without spatial randomness provides another avenue [18]. The presence of strong spin-orbit coupling (SOC) and its effect on the NFL state has also been studied by a model consisting of the Luttinger Hamiltonian supplemented by Coulomb interactions and it was observed that a quantum critical non-Fermi liquid phase can be induced provided time-reversal and cubic symmetries are maintained [19]. In this context, pyrochlore iridates with sizable SOC have largely taken the center stage and systems like $A_2Ir_2O_7$ ($A =$ Pr, Eu) have indeed shown unusual NFL behaviors [19,20].

Experimentally it is possible to identify the NFL systems by probing the transport, thermodynamic, and magnetic behaviors, due to their distinct deviation from standard FL behavior. For example, some of the typical hallmark signatures of NFL are as follows: deviation from quadratic temperature dependence of resistivity, $\rho \sim T^n (1 \leqslant n \leqslant 2)$, logarithmic dependence in low temperature heat capacity, power law ($\chi \sim T^{-p}$; $p < 1$) or logarithmic dependence of magnetic susceptibility $\chi(T)$, etc., and iridates, possessing a complex interplay between intra-atomic Coulomb repulsion energy (U), non-cubic crystal field energy (Δ^{CFE}), intrasite hopping (t), and most importantly spin-orbit coupling (λ) [1,21–23] within

their electronic structure, could gather maximum interest in this context, due to the experimental observation of such deviations, especially in certain members of the pyrochlore family [19,20,24].

Recently, $Pr_2Ir_2O_7$, the metallic member of the pyrochlore family, has been found to exhibit non-Fermi liquid behavior due to three-dimensional quadratic band touching at the Brillouin zone center [19]. However, a general understanding of such NFL state in pyrochlore iridate is still far from complete. Recently the emergence of the NFL state in another pyrochlore iridate, upon hole doping, has also been demonstrated in $Eu_{2-x}Sr_xIr_2O_7$ [20]. The substitution of trivalent Eu by divalent Sr also leads to the suppression of long range magnetic order with simultaneous extension of metallicity down to at least 2 K. This NFL behavior was argued to have arisen due to the disordered distribution of significantly different SOC strengths (λ) of Ir^{4+} and Ir^{5+}, which are generated due to hole doping. It has been mentioned earlier that disorder can indeed lead to a non-Fermi liquid scenario in correlated systems [13,15–18] and even induce metal to insulator transition [25], and therefore, mixed-valent higher transition metals with strong SOC may be considered as a good starting point to investigate the breakdown of Fermi liquid description.

Here we report NFL-like behavior in $Pb_2Ir_2O_{7-\delta}$, another less explored member of the metallic iridate pyrochlore family. In this case, the absence of a rare earth magnetic ion at the A site provides a good opportunity to independently study the physical properties associated with only Ir in this metallic sample. On the other hand, Ir is supposed to be in a $5d^4$ (Ir^{5+}) state in this system with comparatively weaker SOC strength than the tetravalent iridates as the SOC is renormalized in a solid as $\lambda/2S$. However, this unique system accommodates a high degree of oxygen vacancy which gives rise to a mixture of Ir^{4+} (d^5) and Ir^{5+} (d^4) ions even without any intentional electron or hole doping. Naturally, small changes in the structure may drastically influence the magnetic and electronic ground state properties of this compound as Ir^{4+} is magnetic, whereas Ir^{5+} is expected to stabilize in a nonmagnetic $J_{eff} = 0$ ground state within the jj-coupling description. We found that the x coordinate of the oxygen atom in $Pb_2Ir_2O_{7-\delta}$ is 0.325 (x_c should be 0.3125 for ideal nondistorted octahedra) which leads the Ir-O-Ir bond angle to be $134°$, which is the highest among the pyrochlore iridates at room temperature. As a consequence the system is expected to possess large bandwidth due to enhanced effective hybridization and a moderate U+SOC may not be adequate to open a gap, thereby keeping the system metallic down to at least 2 K. Interestingly, the temperature variation of resistivity deviates from conventional quadratic ($\rho \sim T^2$) dependence. Our combined investigation of transport, magnetic, and thermodynamic properties of the system revealed a robust non-Fermi liquid behavior without any long range magnetic order down to 80 mK as confirmed by muon spin resonance (μSR) experiment.

II. EXPERIMENTAL TECHNIQUE

Polycrystalline samples of $Pb_2Ir_2O_{7-\delta}$ were prepared by a conventional solid state reaction method using high purity (> 99.9%) starting materials PbO and IrO_2 (from Sigma Aldrich) in proper ratio. These mixtures were thoroughly ground and pressed into pellets before initial calcination at $800°C$ for 12 h. Finally the as-calcined pellet was annealed at $900°C$ three times for 12 h each in the oxygen atmosphere with intermediate grindings. The samples were annealed in oxygen atmosphere to avoid any vacancy due to external factors. The phase purity of the sample was checked from x-ray powder diffraction measured using a Rigaku SmartLab x-ray diffractometer with Cu $K\alpha$ radiation at room temperature as well as low temperature down to 4 K. The crystal structure of this sample was obtained after refining the x-ray diffraction (XRD) data by Rietveld technique using the FULLPROF program [26]. Temperature dependent electrical resistivity at zero field and 5 T field was measured using the four probe technique with a Quantum Design PPMS (physical properties measurement system). The x-ray photoelectron spectroscopy (XPS) measurements were carried out using an OMICRON electron spectrometer, equipped with a SPHERA Scienta Omicron analyzer and Al $K\alpha$ monochromatic source with an energy resolution of 0.5 eV. Before collecting the spectra the surface of the pelletized sample was cleaned *in situ* by argon sputtering. The collected spectra were then processed and analyzed with the KOLXPD program. The Ir L_3 and L_2 edge (∼11.2 keV) x-ray absorption spectroscopy (XAS) experiment at ambient temperature was performed in transmission geometry at the XAFS beamline of the Elettra synchrotron radiation facility in Italy [27]. The incident energy was set using a Si(111) double crystal monochromator where a couple of mirrors are used for efficient harmonic suppression. The collected XAS data were processed and analyzed using the freely available DEMETER package [28,29] (ATHENA) and FITYK [30] software. The temperature and magnetic field dependent dc magnetization was carried out using a Quantum Design (superconducting quantum interference device) magnetometer. Heat capacity in zero field was measured using the heat capacity attachment of a Quantum Design PPMS. μSR experiments were performed using the MuSR spectrometer at the ISIS facility in UK.

III. RESULTS AND DISCUSSIONS

XRD pattern obtained from polycrystalline $Pb_2Ir_2O_{7-\delta}$ at different temperatures are refined by Rietveld method, confirming pure single phase with the cubic $Fd\bar{3}m$ space group throughout the temperature range (4–300 K). No anomaly in lattice parameters and/or lifting of crystal symmetry are found, which is consistent with the previous temperature dependent powder neutron diffraction study of Retuerto *et al.* [31]. The best fitted Rietveld refined curve and the collected XRD spectrum at 4 K is shown in Fig. 1(a). The detailed crystal structure parameters are given in the Supplemental Material [32]. The refined crystal structure at room temperature is shown in Fig. 1(b). The structure shows that the Ir atoms form a network of corner shared IrO_6 octahedra while Ir and Pb also form corner shared tetrahedral networks individually (not shown). The structure also forms an edge shared tetrahedral network between $O'Pb_4$ and OPb_2Ir_2 tetrahedra [Fig. 1(c)], i.e., all of these triangular networks contribute to strong inherent geometric frustration in this system. The IrO_6 octahedra are trigonally distorted [see Fig. 1(d)] in the structure. Interestingly, the system happens to have a mixture of Ir^{4+} and Ir^{5+} states due to the tolerance of vacancy at the
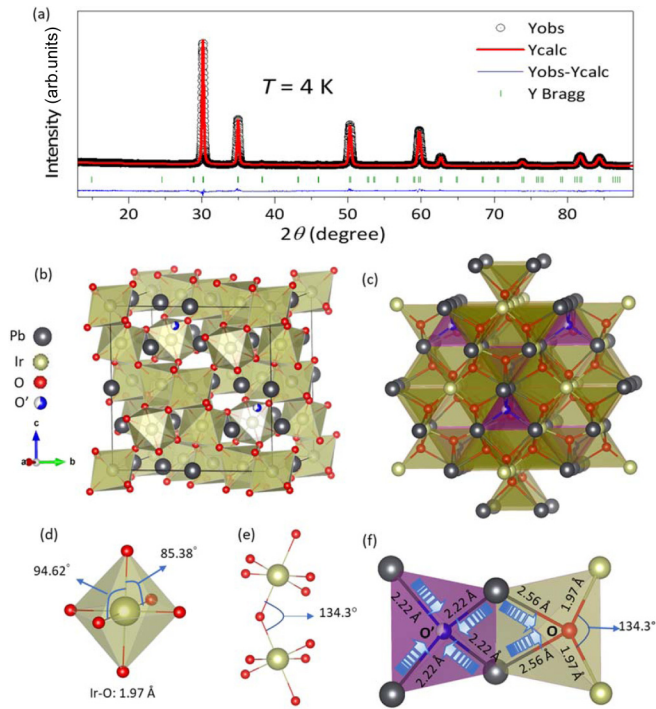
FIG. 2. (a) Ir $4f$ core level XPS spectrum (shaded black circles) along with the fitting (red solid line), showing the contribution of Ir^{5+} (green) and Ir^{4+} (blue), respectively. (b) Oxygen $1s$ spectra showing contribution from O and O′$1s$ level.

O′ site. To avoid any oxygen off-stoichiometry due to a lack of oxygen during synthesis we annealed the sample in O_2 flow at 900 °C. Nonetheless our XRD refinement confirms vacancy at the O′ site in the sample, which proves that the presence of oxygen vacancy is unavoidable in this system. The stereochemically active Pb $6s^2$ lone pair remains directed towards the O′ ion within the O′Pb_4 tetrahedral network through strong hybridization with the O $2p$ orbital [33] which pushes the O′ ion, occupying the $8b$ site, equally from four directions [see Fig. 1(f)] [34]. Therefore to energetically stabilize itself, the system tolerates some vacancy at the O′ site which leads to the formation of the mixture of Ir^{4+} and Ir^{5+} in the system. From XRD refinement the occupancy of the O′ site indicates the value of δ to be 0.48, which is consistent with the neutron powder diffraction study [31]. The charge state in all iridate systems is of central importance as the higher charge state Ir^{5+} carries no magnetic moment and should possess a $J_{eff} = 0$ state in the strong spin-orbit coupled limit (jj coupling) or a magnetic state in the L-S coupling limit depending on the strength of the SOC, whereas Ir^{4+} is magnetic and found to exhibit a spin-orbit coupled $J_{eff} = 1/2$ state commonly reported in insulating iridates. To verify the possible mixed valency of Ir, the photoelectron spectra of Ir $4f$ core level along with O $1s$ level spectra were collected. The distinctively asymmetric shape of the doublet Ir $4f$ core level spectrum [Fig. 2(a)] clearly reveals the presence of two oxidation states of Ir. The spectrum could be fitted with two doublets having
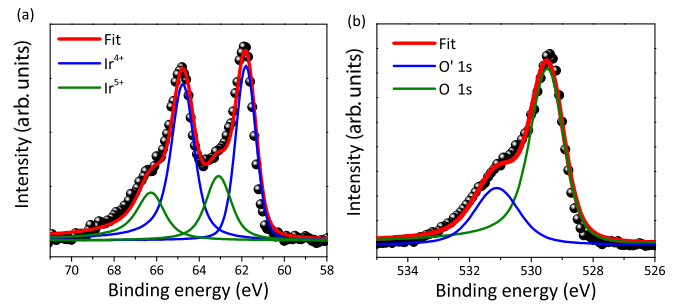
spin-orbit separation of 3.05 and 3.17 eV which confirms the presence of both Ir^{4+} and Ir^{5+} in the system, consistent with previous findings [35,36]. The contribution of Ir^{4+} is approximately twice the contribution of Ir^{5+} in the system, which is somewhat consistent with the oxygen vacancy concentration, but still could be partly erroneous due to the well-known surface effect of the XPS. On the other hand, Pb remains in a $2+$ charge state [37] (see Supplemental Material Fig. S2) as indicated by the binding energy of the $4f$ core level XPS spectra ($4f_{7/2}$-137.2 eV) with a spin-orbit coupling separation of 4.85 eV. The oxygen $1s$ spectra [Fig. 2(b)] can also be clearly seen to consist of two distinct oxygen sites, corresponding to O $1s$ (529.45 eV) with higher intensity and possibly the O′ $1s$ level (531.14 eV) having lower intensity.

Although there are numerous $4d$ itinerant electron systems exhibiting intriguing quantum phenomena, e.g., p-wave superconductivity in Sr_2RuO_4 [38], a field-tuned electronic phase in $Sr_3Ru_2O_7$ [39], itinerant ferromagnetism in $SrRuO_3$ [40], and bad metallicity observed in $CaRuO_3$ [41], it is rare to find itinerant characteristics, although expected, among $5d$ iridates. Most of the iridate systems are found to be insulating due to the complex cooperation between strong spin-orbit coupling and electron-electron correlation (U) [1,42,43], which work together to split the wide $5d$ band and open a gap [left side of Fig. 3, panel (c)]. Interestingly, there have been few examples which behave otherwise. The presence of finite density of states at the Fermi level at room temperature in the XPS valence band spectrum, as seen in Fig. 3(a), confirms that $Pb_2Ir_2O_{7-\delta}$ also falls into that rare category. This metallic nature warrants investigation about the strength of λ in the system. A measure of strength of SOC might give some idea about the bandwidth of the $5d$ level and also about the magnetism of the system. In order to quantify the same, XAS data were collected at the Ir L_2 ($2p_{1/2} \rightarrow 5d$) and L_3 ($2p_{3/2} \rightarrow 5d$) edges [see Fig. 3(b)]. By calculating the relative enhancement of the L_3 edge compared to the L_2 edge it becomes possible to comment on the strength of the spin-orbit coupling of a system [44]. This quantification is defined by the branching ratio, represented as BR = Ir_{L3}/Ir_{L2}. In a single particle picture, without the effect of SOC, the $J_{eff} = 5/2$ and $J_{eff} = 3/2$ states of the Ir $5d$ valence state should be degenerate. Consequently the transition probability to the $5d$ valence state from core $2p$ level will only give rise to the expected statistical branching ratio which is $Ir_{L3}/Ir_{L2} = 2$. Figure 3(b) shows the Ir_{L3}
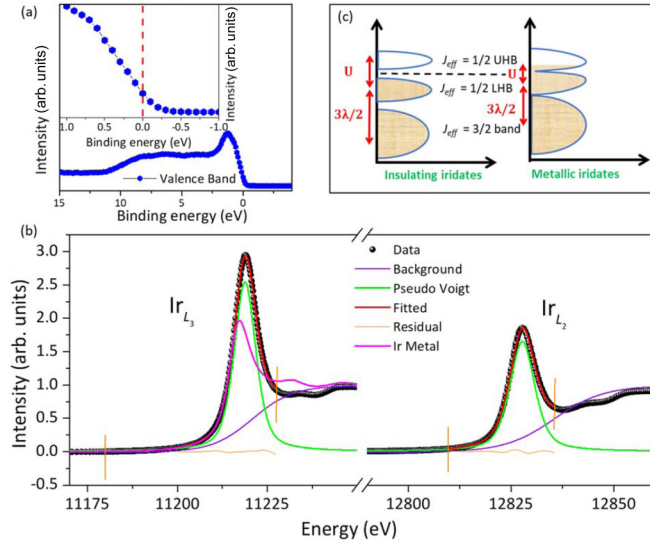
FIG. 3. (a) XPS valence band spectra of the $Pb_2Ir_2O_{7-\delta}$ system. Inset: Zoomed view of spectra near Fermi level. (b) Normalized Ir_{L3} and Ir_{L2} edge white line spectra (shaded black circles) along with the pure metal Ir_{L3} edge spectra (magenta solid line). (c) Schematic diagram of Ir 5d level splitting in the presence of U and SOC.
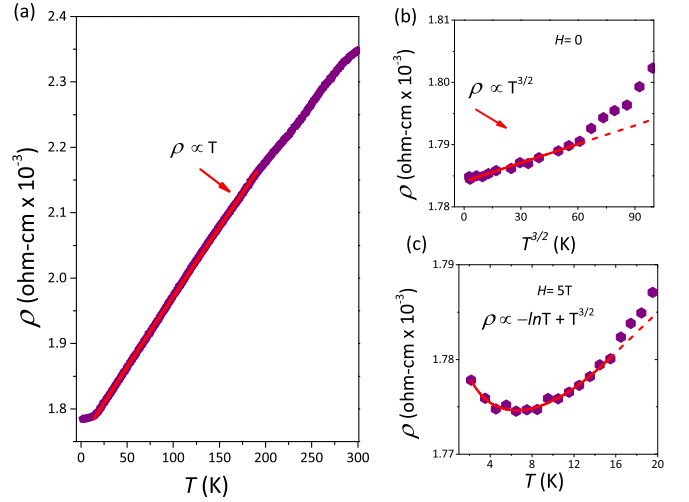

FIG. 4. (a) Linear fitting of resistivity data below 200 K down to 15 K. (b) Low temperature fitting of zero field resistivity data. (c) Low temperature fitting of 5 T field resistivity data.

and Ir_{L2} white line spectra with the corresponding fittings yielding a branching ratio of 2.99 which is clearly higher but significantly smaller than similar iridate oxide systems measured recently and slightly higher than the pure iridium metal [45,46]. Laan and Thole proposed that this branching ratio can be used to relate the expectation value of the spin-orbit operator, $\langle LS \rangle$ by $BR = (2+r)/(1-r)$ where $r = \langle LS \rangle / \langle n_h \rangle$ and $\langle n_h \rangle$ is the average number of holes in the 5d level [47]. Several earlier reports revealed a shift of 1.85–1.9 eV between pure Ir metal (Ir^0) and IrO_2 (Ir^{4+}) which amounts to an average shift of 0.46–0.47 eV per Ir valence state [48,49]. In the present case, a shift of 2 eV is observed [see Fig. 3(b)] between pure Ir metal and $Pb_2Ir_2O_{7-\delta}$ which indicates an average valence state of 4.33 for Ir, i.e., roughly 1/3 of Ir ions in this compound is in Ir^{5+} charge similar to what was observed from XPS analysis; however, slightly less from XRD analysis. Since XANES is a bulk sensitive technique, we have used it to calculate the average number of holes in this system, which is $\langle n_h \rangle = 5.33$. By this calculation the value of $\langle LS \rangle$ was estimated to be 1.32 ($\hbar^2$), which is also small compared to other iridate oxides but larger than pure Ir metal. The comparatively smaller value of $\langle LS \rangle$ indicates a weaker spin-orbit coupling in the system and probably indicates that it may not be strong enough to lift the degeneracy of the d orbitals [right side of Fig. 3(c)]. This is also supported by the single peak feature of the highly symmetric Ir_{L3} white line which should otherwise be an asymmetric double peak feature corresponding to $2p_{3/2} \rightarrow J_{eff} = 5/2$ and $2p_{3/2} \rightarrow J_{eff} = 3/2$ and also essentially indicates the large bandwidth of the 5d valence level in the system which is consistent with our structural and transport analysis showing metallic behavior throughout the temperature range. The electronic properties of pyrochlore iridates are highly sensitive to the bond angle Ir-O-Ir created between corner shared IrO_6 octahedra [see Fig. 1(e)]. Clearly, the size of the Pb ion ($\langle r \rangle_{Pb} = 1.29$ Å), the highest among

A-site cations of known pyrochlore iridates, plays a vital role in determining its bandwidth (W). The difference between the Ir-O-Ir bond angle between insulating and metallic pyrochlore iridates has been roughly known to be of the order of 2° [50]. In $Pb_2Ir_2O_{7-\delta}$ this trend of increasing Ir-O-Ir bond angle coincides with the metallic nature among pyrochlore iridates [51,52]; as illustrated in Fig. 1(f), the larger Pb cation with its extended 6s orbitals pushes the O ion within the OPb_2Ir_2 tetrahedra towards the Ir ions making the Ir-O-Ir bond angle to be 134°, the largest among the reported pyrochlore iridates, resulting in a shorter Ir-O distance and consequently stronger hybridization of the extended Ir 5d and O 2p orbitals [see Fig. 1(f)] and higher W. Therefore, experiment proves that this system has a moderate λ and also probably a moderate U with a significantly large bandwidth and as a result, metallicity is realized.

However, the temperature dependent resistivity $\rho(T)$ measurement down to 2 K [Fig. 4(a)] offered a surprise. The resistivity remains linear throughout the temperature range down to at least 15 K. The weak feature above 200 K might result due to the tiny structural distortion caused by the non-monotonous decrease of Ir-Ir bonds (see Fig. S1) around similar temperature. Most importantly it follows a $\rho \sim T^{3/2}$ dependence below 15 K down to 2 K (see Fig. 4) contrary to the expected $\rho \sim T^2$ variation, expected for a Fermi liquid system at low temperature. Clearly, the system violates the Fermi liquid behavior of a conventional metallic system. However, its 4d counterpart pyrochlore does follow a conventional Fermi liquid behavior [53] of $\rho \sim T^2$. Surprisingly, even at the application of a 5 Tesla magnetic field the linear temperature dependence of resistivity does not change except for a logarithmic upturn below 15 K and no T^2 dependence emerged signifying a robust nature of the non-Fermi liquid behavior in the system [Fig. 4(c)]. On the other hand, for a standard metal the maximum resistivity is of the order of $\rho_{max} \sim 1$ mΩ cm [54]. As can be seen from Fig. 4(a) the resistivity is larger than the ρ_{max} value even at lowest temperature and it does not saturate even at 300 K ($\rho_{300 K} = 2.4$ mΩ cm).
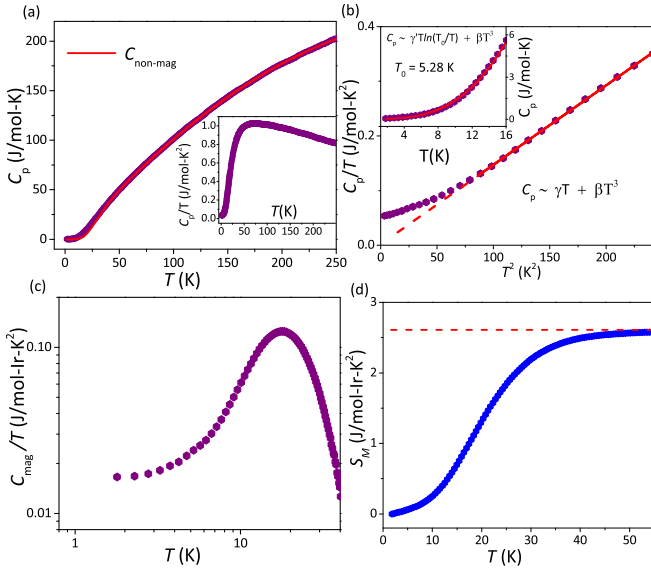
FIG. 5. (a) Temperature dependence of total specific heat C_p (purple sphere) in the whole temperature range along with Debye-Einstein (DE) fitting (red solid line) for lattice contribution at zero field. (b) Deviation of the $C_p = \gamma T + \beta T^3$ nature at low T in C_p/T vs T data; the inset shows the low temperature fitting of C_p vs T data with modified $C_p = \gamma'T \ln(T_0/T) + \beta T^3$. (c) Magnetic contribution C_{mag}/T vs T in logarithmic scale. (d) Magnetic entropy (S_M) release as a function of temperature (dashed red line shows the maximum entropy release).

However, the $4d$ counter part of the system, $Pb_2Ru_2O_6O'$ tends to saturate at room temperature with a maximum resistivity $\rho_{max} \sim 200\ \mu\Omega$ cm. Evidently $Pb_2Ir_2O_{7-\delta}$ behaves more like a *bad metal* rather than a conventional Fermi liquid metal. Such bad metals are often found to violate the Mott-Ioffe-Regal (MIR) limit of maximum resistivity [55] ($l \sim a$, $k_F \sim 1$, where l is the mean free path, a is the lattice parameter, and k_F is the Fermi wave vector) in high T_c cuprate superconductors [14,16], heavy fermions [56], and also recently in some semimetallic pyrochlore iridate systems [20,57], which is indicative of non-Fermi liquid behavior. Violation of MIR is often discussed in the context of disordered solids [58]. Therefore, the non-Fermi liquid behavior could arise in this system due to a disordered distribution of Ir^{4+} and Ir^{5+} ions arising due to the mixed-valent nature of the system which has largely different SOC values unlike in its $4d$ counterpart $Pb_2Ru_2O_6O'$ as it should be noted that in a solid the strength of spin-orbit coupling is renormalized as $\lambda_{eff} = \lambda_{atomic}/2S$ where S is the total spin.

A measure of the heat capacity may give deeper insight into the NFL behavior of the system. Therefore, heat capacity (C_p vs T) was measured down to 1.8 K and displayed in Fig. 5(a). No λ-like anomaly was observed in C_p/T vs T data, confirming the absence of any long range order or any structural phase transition, as confirmed by the XRD analysis of the system. For a Fermi liquid system, low temperature heat capacity (C_p) should be linear along with the weak T^3 lattice term. Therefore, we fitted the low temperature C_p data below 15 K with $C_p = \gamma T + \beta T^3$ where the first part denotes electronic contribution and the latter accounts for lattice contribution.

However, C_p/T vs T^2 strongly deviates below 10 K, which is once again consistent with the deviation from quadratic nature of resistivity ($\rho \sim T^2$) of the system. This gives us roughly the T linear component to be $\gamma = 1.84$ mJ/mol K^2 and $\beta = 1.45$ mJ/mol K^3. The rather low value of γ confirms that there is no perceptible mass enhancement of the fermions in the system. The value of the Sommerfeld coefficient signifies it has a very small area on the Fermi surface consistent with the bad metal characteristic as observed from the resistivity measurements as well. On the other hand, it could be well fitted at low temperature with $C_p = \gamma'T \ln(T_0/T) + \beta T^3$ below 15 K down to 1.8 K as shown in the inset of Fig. 5(b). A logarithmic increase at low temperature is often observed in non-Fermi liquid systems [5,57], and recently it has been also reported in a hole doped pyrochlore system [20]. It might be worth calculating the Wilson ratio here, which is defined as

$$R_W = \frac{4\pi^2 k_B^2 \chi_0}{(g\mu_B)^2 \gamma} \tag{1}$$

yielding a value 21.7, which is way larger than the values evidenced for correlated metals with strong spin-orbit coupling ($R_W \sim 1$–6) [59]. This notably high R_W value is an outcome of the strong non-Fermi liquid nature of the compound, which is consistent with the resistivity analysis. The occurrence of a high R_W value in non-Fermi liquids is not unusual and also been observed in the semimetallic NFL iridate $SrIrO_3$ ($R_W \sim 55$) [57] signifying proximity to a quantum critical point.

Now, the magnetic contribution to the heat capacity can be estimated as $C_{mag} = C_p - C_{nonmag}$, where C_p is the total heat capacity. In the absence of a suitable nonmagnetic analog, the nonmagnetic contribution can be modeled as $C_{nonmag} = C_{latt} + C_{elec}$. To estimate the lattice contribution, a Debye-Einstein equation [$C_{latt} = C(\Theta_{D,E}, T)$] [60] has been used and the electronic contribution is taken as $C_{elec} \sim \gamma T$. The fitting yielded a $\Theta_D \sim 426$ K and $\Theta_E \sim 130, 402$, and 788 K. However, a low temperature heat capacity fitting may lead to a poor estimation of magnetic contribution of the system. Therefore, the total heat capacity C_p was first fitted in the temperature range (55–250 K) and then extrapolated down to 1.8 K [see Fig. 5(a)] and taken as the C_{nonmag}. After subtracting C_{nonmag} from the total C_p, finally, the magnetic heat capacity of the sample was estimated. A broad peak was observed in C_{mag}/T vs T around 20 K which is often observed in spin frustrated systems [61–63]. Nonetheless, the low temperature (< 15 K) C_p being well described by the inclusion of the nonlinear $\gamma'T \ln(T_0/T)$ term, the exact magnetic behavior in this region is difficult to interpret. The magnetic entropy of the system was subsequently calculated by the formula $S_m(T) = \int_0^{T'} C_{mag}/T'$, and the results are displayed in Fig. 5(d). The magnetic entropy release is 2.6 mJ/mol Ir K^2 above 40 K, which is about 40% of $R \ln(2J+1)$ of the $J = 1/2$ for the d^5 Ir ion and almost 25% of the $J = 1$ for the d^4 Ir ion. The retention of large magnetic entropy at low temperature also indicates the highly frustrated nature of the Ir ions in this pyrochlore system, which forbids any long range magnetic ordering.

To further understand the NFL behavior we have performed magnetic measurements on the system down to 2 K.
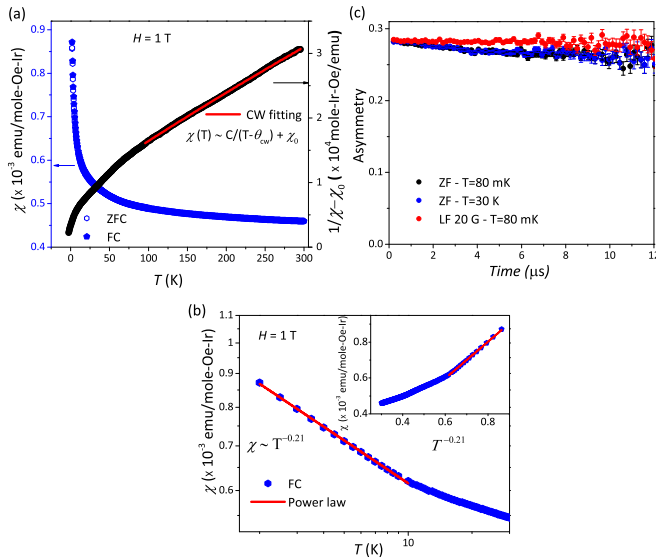
FIG. 6. (a) Left axis (blue): Temperature dependent dc susceptibility variations during zero field cooled (open blue circles) and field cooled (shaded blue circles) protocols, Right axis (black): Temperature dependence of $1/(\chi - \chi_0)$ is plotted with Curie-Weiss fitting (red solid line). (b) Log-log plot of low temperature magnetic susceptibility data (blue solid circle) and fitted curve (red solid line). Inset: χ vs $T^{-0.21}$ plot and linear fitting (solid red line). (c) Time evolution of zero field μSR spectra at 80 mK and at 30 K and longitudinal field (20 Oe) spectra at 80 mK.

Figure 6(a) shows the temperature dependence of the dc magnetic susceptibility (χ vs T) down to 2 K, measured in zero field cooled (ZFC) and field cooled (FC) protocols. Having a metallic characteristic down to 2 K, it was expected to be a Pauli paramagnet like IrO_2; however, it deviates strongly as a strong upward Curie turn at low temperature is observed. No sign of long range magnetic order down to 2 K is observed in this nearly featureless paramagneticlike behavior suggesting a continuation of the spin fluctuation of Ir ions in the system, unlike other d^5 [51,64,65] pyrochlore iridates except $Pr_2Ir_2O_7$, which shows small spin freezing at very low temperature [66]. We have analyzed the susceptibility (in an applied field of 10 kOe) data using the Curie-Weiss (C-W) equation $\chi = \frac{C}{T - \Theta_{CW}} + \chi_0$ (C is the Curie constant while Θ_{CW} and χ_0 represent the Curie-Weiss temperature and the temperature independent susceptibility, respectively) in the temperature range 100–300 K as shown in Fig. 6(a). The fitting yielded a strong negative Θ_{CW} value of around -96 K and an effective magnetic moment of $\mu_{\text{eff}} \sim 0.3\mu_B$/Ir. The large negative Θ_{CW} of -96 K indicates a strong nearest neighbor antiferromagnetic interaction, but the absence of any magnetic ordering suggests the presence of inherent geometric frustration in the system expected in a pyrochlore lattice. The closest analog of the present system in terms of the nonmagnetic A-site cationic radius, $Bi_2Ir_2O_7$, where Ir is almost entirely present in a 4^+ charge state, also poses metallicity but with strong ferromagnetic instability and the emergence of saturation in magnetic moments vs field data, unlike the present case. Clearly, while $Bi_2Ir_2O_7$ is on the verge of long range magnetic order ($\Theta_{CW} \sim -2$ K) [67], $Pb_2Ir_2O_{7-\delta}$

remains far from ordering at least down to 2 K. Therefore, even if pyrochlore iridates are expected to be in *all-in-all-out* (AIAO) magnetic ground state at low temperature, $Pb_2Ir_2O_{7-\delta}$ becomes another exception in the pyrochlore family where frustration seems to dominate. Random distribution of Ir^{4+} and Ir^{5+} ions in the system, which can be thought of as a disorder, may also act against any long range magnetic ordering. On the other hand, the divergence of magnetic susceptibility below 10 K [see Fig. 6(b)] takes a power law form of $\chi \sim T^{-\alpha}$ ($\alpha \sim 0.21$) which is a typical characteristic of non-Fermi liquids [5], consistent with our transport analysis. Even under the field of 4 T, the low temperature χ retains its power dependence [32] with a slightly higher value of $\alpha = 0.23$ compared to the 1 T data, unlike the NFL $SrIrO_3$ [57]. However, in the 4 T data the power law fitting could only be done at a smaller temperature range (< 7 K). Although the $SrIrO_3$ has been found to reside near a quantum critical point (QCP) ($T = 0$ and $\mu_0 H = 0.23$ T) where the low temperature magnetic susceptibility exponent is highly sensitive to very low applied magnetic fields indicating a ferromagnetic instability in the system, this is not the case for the present system. Therefore, $Pb_2Ir_2O_{7-\delta}$ shows the robustness of the NFL characteristic and the quantum critical point could not be realized down to 2 K and at high field. One should note that $SrIrO_3$ is a purely stoichiometric compound, whereas $Pb_2Ir_2O_{7-\delta}$ has oxygen off-stoichiometry leading to the distribution of Ir^{4+} and Ir^{5+} in the system.

To get more insight into the spin dynamics, local magnetic probe muon spin relaxation has been performed. The temperature dependent μSR spectra between 80 mK and 30 K at zero field is shown in Fig. 6(c). However, no signature of oscillation was observed down to at least 80 mK, confirming the absence of long range magnetic order which implies the preservation of the time-reversal symmetry in the system. Contrary to the anticipated AIAO magnetic configuration where all of the spins of magnetic ions point either inward or outward with respect to the center of the tetrahedra [68,69], the disordered distribution between Ir^{4+} and Ir^{5+} may hinder the long range magnetic order in the present system. In the hole doped pyrochlore iridate system $Eu_{2-x}Sr_xIr_2O_7$ [20] the NFL state was observed with the simultaneous suppression of magnetic order. This is in line with the theoretical claim by Moon *et al.* [19] which predicts non-Fermi liquid state in pyrochlore iridates provided time-reversal and cubic symmetries are protected.

One can also calculate the frustration parameter $f_N = \Theta_{CW}/T_N$ (T_N is the lowest probed temperature) from the C-W fit in the magnetic susceptibility measurement, which comes out to be as large as 1200. Nonetheless, the extremely slow relaxation nature of muon spin is somewhat surprising given the strong geometric frustration in the system. The relaxation does not evolve with temperature, as the signal remains almost similar between 80 mK and 30 K (in-between temperatures not shown). This signifies the complete absence of freezing of Ir moments down to at least 80 mK. Evidently the system stays in a fast fluctuating paramagnetic limit in the whole temperature limit. Upon application of a mere 20 Oe longitudinal field the feeble relaxation completely dies off. The weak decoupling nature of muon spins signifies the nature of relaxation is static originating from nuclei moments [70].

However, one should take note that only 20% of Pb bears a nuclear spin [71], and the one on Ir is super small. On the other hand, the muons stop far from these 20% Pb nuclear spin near Ir moments which are very small. Clearly this weak relaxation arises due to weak dipolar Pb nuclear interaction and small Ir moments.

IV. SUMMARY AND CONCLUSION

In summary we have demonstrated that $Pb_2Ir_2O_{7-\delta}$ is a weakly correlated metal with moderate SOC and mixed Ir valency that exhibits unusual electronic transport, magnetic, and thermodynamics properties that deviate from the normal Fermi liquid behaviors. The linear temperature dependence in resistivity over a large temperature range and typical $T^{3/2}$ dependence below 15 K is observed by experiment. On the other hand, the magnetic contribution at low T follows a power law behavior which is retained even under a strong field and indicates the onset of a non-Fermi liquid state in the system. The μSR and magnetic susceptibility data discarded any sign of long range magnetic ordering in the system down to at least 80 mK. The random distribution between Ir^{4+} and Ir^{5+} which can be thought of as disorder may prevent the system from being ordered. Strong inherent geometric frustration (frustration parameter $f_N \sim 1200$) is also prevalent in the system. Despite having metallicity down to the lowest measured temperature it shows a very small Sommerfeld coefficient in the low temperature heat capacity fitting, signifying small density of low energy excitations at Fermi level, and

consequently a large Wilson ratio ($R_W \sim 22$) asserting its robust non-Fermi liquid nature. The absence of a magnetic ion at the A site and a very low value of the Sommerfeld coefficient (T linear term in heat capacity), strongly disregards the Kondo mechanism as being responsible for the observed NFL nature in the system. Also there is no sign of Kondo resistivity in the sample. Our analysis does not find the proximity to the QCP. However, a pressure dependent study might be very useful for a deeper understanding of the emergence of the NFL phenomenon in pyrochlore iridates. The non-Fermi liquid behavior in $Pb_2Ir_2O_{7-\delta}$ could be ascribed to the disordered distribution of Ir^{4+} and Ir^{5+} which has different strengths of spin-orbit coupling. Therefore locally there could be largely different coupling due to the distribution of d^4 ($S = 1$) and d^5 ($S = 1/2$) ions. Nonetheless, this NFL phenomenon in pyrochlore iridates adds to the myriad of complex electronic and magnetic ground states it hosts.

[1] B. J. Kim, H. Jin, S. J. Moon, J. Y. Kim, B. G. Park, C. S. Leem, J. Yu, T. W. Noh, C. Kim, S.-J. Oh *et al.*, Phys. Rev. Lett. **101**, 076402 (2008).

[2] X. Wan, A. M. Turner, A. Vishwanath, and S. Y. Savrasov, Phys. Rev. B **83**, 205101 (2011).

[3] S. Nakatsuji, K. Kuga, Y. Machida, T. Tayama, T. Sakakibara, Y. Karaki, H. Ishimoto, S. Yonezawa, Y. Maeno, E. Pearson *et al.*, Nat. Phys. **4**, 603 (2008).

[4] A. J. Millis, Phys. Rev. B **48**, 7183 (1993).

[5] V. K. Anand, D. T. Adroja, A. D. Hillier, K. Shigetoh, T. Takabatake, J.-G. Park, K. A. McEwen, J. H. Pixley, and Q. Si, J. Phys. Soc. Jpn. **87**, 064708 (2018).

[6] M. Z. Hasan and C. L. Kane, Rev. Mod. Phys. **82**, 3045 (2010).

[7] K. M. Shen and J. S. Davis, Mater. Today **11**, 14 (2008).

[8] Y. M. Dai, H. Miao, L. Y. Xing, X. C. Wang, P. S. Wang, H. Xiao, T. Qian, P. Richard, X. G. Qiu, W. Yu *et al.*, Phys. Rev. X **5**, 031035 (2015).

[9] M. A. Metlitski and S. Sachdev, Phys. Rev. B **82**, 075128 (2010).

[10] M. A. Metlitski, D. F. Mross, S. Sachdev, and T. Senthil, Phys. Rev. B **91**, 115111 (2015).

[11] S. Raghu, G. Torroba, and H. Wang, Phys. Rev. B **92**, 205104 (2015).

[12] S. Lederer, Y. Schattner, E. Berg, and S. A. Kivelson, Phys. Rev. Lett. **114**, 097001 (2015).

[13] Y. Wang, Phys. Rev. Lett. **124**, 017002 (2020).

[14] A. J. Schofield, Contemp. Phys. **40**, 95 (1999).

[15] M. Milovanović, S. Sachdev, and R. N. Bhatt, Phys. Rev. Lett. **63**, 82 (1989).

[16] G. R. Stewart, Rev. Mod. Phys. **73**, 797 (2001).

[17] E. Miranda and V. Dobrosavljević, Rep. Prog. Phys. **68**, 2337 (2005).

[18] I. Esterlis, H. Guo, A. A. Patel, and S. Sachdev, Phys. Rev. B **103**, 235129 (2021).

[19] E.-G. Moon, C. Xu, Y. B. Kim, and L. Balents, Phys. Rev. Lett. **111**, 206401 (2013).

[20] A. Banerjee, J. Sannigrahi, S. Giri, and S. Majumdar, Phys. Rev. B **96**, 224426 (2017).

[21] W. Witczak-Krempa, G. Chen, Y. B. Kim, and L. Balents, Annu. Rev. Condens. Matter Phys. **5**, 57 (2014).

[22] D. Pesin and L. Balents, Nat. Phys. **6**, 376 (2010).

[23] B. J. Kim, H. Ohsumi, T. Komesu, S. Sakai, T. Morita, H. Takagi, and T. Arima, Science **323**, 1329 (2009).

[24] T. Kondo, M. Nakayama, R. Chen, J. J. Ishikawa, E.-G. Moon, T. Yamamoto, Y. Ota, W. Malaeb, H. Kanai, Y. Nakashima *et al.*, Nat. Commun. **6**, 10042 (2015).

[25] V. Dobrosavljević and G. Kotliar, Phys. Rev. Lett. **78**, 3943 (1997).

[26] J. Rodriguez Carvajal, Phys. B: Condens. Matter **192**, 55 (1993).

[27] A. Di Cicco, G. Aquilanti, M. Minicucci, E. Principi, N. Novello, A. Cognigni, and L. Olivi, J. Phys.: Conf. Ser. **190**, 012043 (2009).

[28] M. Newville, J. Synchrotron Radiat. **8**, 322 (2001).

[29] B. Ravel and M. Newville, J. Synchrotron Radiat. **12**, 537 (2005).

[30] M. Wojdyr, J. Appl. Cryst. **43**, 1126 (2010).

[31] M. Retuerto, T. Sarkar, M.-R. Li, A. Ignatov, M. Croft, J. P. Hodges, T. Thao Tran, P. Shiv Halasyamani, and M. Greenblatt, Mater. Res. Express **1**, 046304 (2014).

[32] See Supplemental Material at http://link.aps.org/supplemental/10.1103/PhysRevB.105.085137 for detailed XRD refined parameters.

[33] R. Ali Saha, A. Halder, T. Saha-Dasgupta, D. Fu, M. Itoh, and S. Ray, Phys. Rev. B **101**, 180406(R) (2020).

[34] H.-J. Koo, M.-H. Whangbo, and B. J. Kennedy, J. Solid State Chem. **136**, 269 (1998).

[35] H. Kumar, R. S. Dhaka, and A. K. Pramanik, Phys. Rev. B **95**, 054415 (2017).

[36] B. J. Kennedy, J. Solid State Chem. **123**, 14 (1996).

[37] D. J. Payne, R. G. Egdell, W. Hao, J. S. Foord, A. Walsh, and G. W. Watson, Chem. Phys. Lett. **411**, 181 (2005).

[38] Y. Maeno, H. Hashimoto, K. Yoshida, S. Nishizaki, T. Fujita, J. G. Bednorz, and F. Lichtenberg, Nature (London) **372**, 532 (1994).

[39] S. A. Grigera, R. P. Perry, A. J. Schofield, M. Chiao, S. R. Julian, G. G. Lonzarich, S. I. Ikeda, Y. Maeno, A. J. Millis, and A. P. Mackenzie, Science **294**, 329 (2001).

[40] M. Kim and B. I. Min, Phys. Rev. B **91**, 205116 (2015).

[41] G. Cao, W. H. Song, Y. P. Sun, and X. N. Lin, Solid State Commun. **131**, 331 (2004).

[42] G. Khaliullin, Phys. Rev. Lett. **111**, 197201 (2013).

[43] O. N. Meetei, W. S. Cole, M. Randeria, and N. Trivedi, Phys. Rev. B **91**, 054412 (2015).

[44] B. T. Thole and G. van der Laan, Phys. Rev. B **38**, 3158 (1988).

[45] J. P. Clancy, N. Chen, C. Y. Kim, W. F. Chen, K. W. Plumb, B. C. Jeon, T. W. Noh, and Y.-J. Kim, Phys. Rev. B **86**, 195131 (2012).

[46] E. Zoghlin, Z. Porter, S. Britner, S. Husremovic, Y. Choi, D. Haskel, G. Laurita, and S. D. Wilson, J. Phys.: Condens. Matter **33**, 055601 (2021).

[47] G. van der Laan and B. T. Thole, Phys. Rev. Lett. **60**, 1977 (1988).

[48] X. Zhenga, J. Tanga, A. Galloc, J. A. Garrido Torresc, X. Yua, C. J. Athanitisa, E. M. Beena, P. Ercius *et al.*, Proc. Natl. Acad. Sci. USA **118**, e2101817118 (2021).

[49] H. N. Nong, T. Reier, H.-S. Oh, M. Gliech, P. Paciok, T. H. T. Vu, D. Teschner, M. Heggen,

V. Petkov, R. Schlögl *et al.*, Nat. Catal. **1**, 841 (2018).

[50] M. D. Field, B. J. Kennedy, B. A. Hunter, and T. Vogt, J. Solid State Chem. **144**, 467 (1999).

[51] K. Matsuhira, M. Wakeshima, R. Nakanishi, T. Yamada, A. Nakamura, W. Kawano, S. Takagi, and Y. Hinatsu, J. Phys. Soc. Jpn. **76**, 043706 (2007).

[52] D. Yanagishima and Y. Maeno, J. Phys. Soc. Jpn. **70**, 2880 (2001).

[53] P. Zheng, N. L. Wang, J. L. Luo, R. Jin, and D. Mandrus, Phys. Rev. B **69**, 193102 (2004).

[54] N. E. Hussey II, K. Takenaka, and H. Takagi, Philos. Mag. **84**, 2847 (2004).

[55] N. F. Mott, *Metal-Insulator Transitions* (Taylor & Francis, London/Philadelphia, 1990).

[56] M. B. Maple, Phys. B: Condens. Matter **215**, 110 (1995).

[57] G. Cao, V. Durairaj, S. Chikara, L. E. DeLong, S. Parkin, and P. Schlottmann, Phys. Rev. B **76**, 100402(R) (2007).

[58] P. P. Edwards, M. T. J. Lodge, F. Hensel, and R. Redmer, Philos. Trans. R. Soc. A **368**, 941 (2010).

[59] L. E. DeLong, R. P. Guertin, S. Hasanain, and T. Fariss, Phys. Rev. B **31**, 7059 (1985).

[60] M. S. Khan, A. Bandyopadhyay, A. Nag, V. Kumar, A. V. Mahajan, and S. Ray, Phys. Rev. B **100**, 064423 (2019).

[61] Y. Okamoto, M. Nohara, H. Aruga-Katori, and H. Takagi, Phys. Rev. Lett. **99**, 137207 (2007).

[62] L. Balents, Nature (London) **464**, 199 (2010).

[63] J. G. Cheng, G. Li, L. Balicas, J. S. Zhou, J. B. Goodenough, C. Xu, and H. D. Zhou, Phys. Rev. Lett. **107**, 197204 (2011).

[64] M. J. Lawler, A. Paramekanti, Y. B. Kim, and L. Balents, Phys. Rev. Lett. **101**, 197202 (2008).

[65] N. Taira, M. Wakeshima, and Y. Hinatsu, J. Phys.: Condens. Matter **13**, 5527 (2001).

[66] S. Nakatsuji, Y. Machida, Y. Maeno, T. Tayama, T. Sakakibara, J. van Duijn, L. Balicas, J. N. Millican, R. T. Macaluso, and J. Y. Chan, Phys. Rev. Lett. **96**, 087204 (2006).

[67] P. J. Baker, J. S. Möller, F. L. Pratt, W. Hayes, S. J. Blundell, T. Lancaster, T. F. Qi, and G. Cao, Phys. Rev. B **87**, 180409(R) (2013).

[68] C. Donnerer, M. C. Rahn, M. M. Sala, J. G. Vale, D. Pincini, J. Strempfer, M. Krisch, D. Prabhakaran, A. T. Boothroyd, and D. F. McMorrow, Phys. Rev. Lett. **117**, 037201 (2016).

[69] S.-K. Jian and W. Nie, Phys. Rev. B **97**, 115162 (2018).

[70] F. Bert, Collection SFN **13**, 03001 (2014).

[71] R. J. Snodgrass and L. H. Bennett, Phys. Rev. **132**, 1465 (1963).